

## A Lamb wave scanning approach for the mapping of defects in [0/90] titanium matrix composites

T. Kundu <sup>a,\*</sup>, K. Maslov <sup>b</sup>, P. Karpur <sup>c</sup>, T.E. Matikas <sup>c</sup>, P.D. Nicolaou <sup>d</sup>

<sup>a</sup> Department of Civil Engineering and Engineering Mechanics, University of Arizona, Tucson, AZ 85721, USA

<sup>b</sup> Semenov Institute of Chemical Physics, Russian Academy of Science, Moscow 117334, Russia

<sup>c</sup> Research Institute, University of Dayton, 300 College Park Avenue, Dayton, OH 45469-0127, USA

<sup>d</sup> Systran Corporation, Linden Avenue, Dayton, OH 45432, USA

Received 8 December 1994; Revised 6 November 1995

### Abstract

In this paper a new scanning technique using leaky Lamb waves is presented. This technique is applied to detect internal defects in a multilayered fiber-reinforced composite plate specimen (SCS-6 fibers in Ti-6Al-4V matrix). Images generated by this new Lamb wave scanning technique (we will refer it as the L-scan technique) are compared with conventional C-scan images. This comparison shows that the L-scan technique is more effective for detecting some internal defects such as missing fibers and fiber breakage type defects in a multilayered specimen than the conventional C-scan technique.

**Keywords:** Lamb wave scanning; Acoustic image; Composite plates

### 1. Introduction

The ultrasonic technique has become one of the most popular nondestructive testing techniques because of its versatility and ease of operation. It can detect internal cracks and inclusion-type defects in homogeneous or layered materials, most of the time, without much difficulty. However, the conventional scanning technique has its own shortcomings. It is not very effective in detecting cracks that are vertical to the plate surface. This is because the ultrasonic signal is not reflected by the crack when the signal propagation direction is parallel to the crack surface. The back scattering technique and acoustic microscopy technique are used for detecting such vertical defects. However, when these defects are not located very close to the surface these techniques also encounter difficulties. Use of Lamb waves to detect such defects may be a viable alternative to the currently practised methods. Theoretical studies by Kundu and Blodgett [1], Yang and Kundu [2,3] and Yang [4] have shown that different Lamb wave modes produce different levels of excitation in various layers in a multilayered solid

plate. This phenomenon is exploited here to generate experimentally C-scan images of different layers of a composite plate by propagating Lamb waves of different modes through the plate. The C-scan image generated by receiving the leaky Lamb waves is denoted as the 'L-scan' image in this paper.

Previous efforts of using leaky waves to inspect defects in composite and metal plates include the works of Chimenti and Nayfeh [5], Nagy et al. [6], Pearson and Murri [7], Rose et al. [8], Nayfeh [9], Bar-Cohen and Chimenti [10], Chimenti and Bar-Cohen [11], Martin and Chimenti [12], Mal and Bar-Cohen [13], Chimenti and Martin [14], Bar-Cohen and Chimenti [15], Chimenti and Fielder [16], Ditri and Rose [17] among others. Most of these works involve relating the material defects such as the porosity and delamination to the change in the Lamb wave propagation characteristics, the dispersion curves, phase velocity and attenuation. Not many investigators have attempted to scan the specimen using Lamb waves to generate the L-scan image. Chimenti and Martin [14] however, did it with some success. They positioned the transmitter and the reflector in a pitch-catch arrangement over the specimen to generate leaky Lamb waves. They placed the receiver

\* Corresponding author. Fax: +1-602-621-2550.

in the null zone and scanned the specimen. The null zone position changes in the presence of an internal defect. Hence, when a defect is encountered the receiver voltage amplitude is altered and the image of the defect is generated. The major problem with this arrangement is that the null zone position is very sensitive to the plate thickness. Hence, a few percent change in the plate thickness alters the receiver voltage amplitude significantly. To avoid this problem one needs to filter the L-scan generated data through a special filter, called a Mfq filter [14]. This signal processing helps to minimize the effect of the plate thickness variation on the null zone but retains the sensitivity to defects of interest.

In this paper, the problem imposed by the slight variation in plate thickness, is avoided by placing the receiver beyond the null zone and the specularly reflected zone. Thus, only propagating leaky Lamb waves are received by the receiver. During our experiment we found that the propagating Lamb wave amplitudes for some modes are comparatively less sensitive to the plate thickness variation. If we scan the specimen with these Lamb wave modes then the need for using the Mfq filter does not arise. Banik et al. [18] also found that some Rayleigh–Lamb modes are less sensitive to the layer thickness variation than others.

## 2. Methodology

The first step in generating an L-scan image is to produce propagating Lamb waves in the specimen. For this purpose two transducers are positioned in a pitch-catch arrangement over the plate specimen as shown in Fig. 1. The transmitter is excited by the tone burst excitation. The excitation frequency is then varied continuously from a minimum value to a maximum value within the band width of the transducers. The reflected signal is received by the receiver, the signal amplitude is then displayed on an oscilloscope screen as a function of the frequency. When the transmitters and the reflector are positioned such that the reflected energy is maximum or very close to maximum then the reflected amplitude spectrum has shapes as shown in Figs. 1a or 1b. If no Lamb waves are generated then the spectrum looks like the plot shown in Fig. 1a, which has been generated by a couple of broadband 5 MHz transducers taking an aluminum block as the reflector, thus no Lamb waves are excited in the specimen. However, if leaky Lamb waves are generated at some frequencies, then at those frequencies dips are observed, as shown in Fig. 1b, which is produced by the same set of transducers at the same orientation but the aluminum block is replaced by a thin composite plate, where Lamb waves are excited at some frequencies. If the transducers are moved further down, i.e. the specimen-transducer distance is reduced without altering the distance between the two trans-

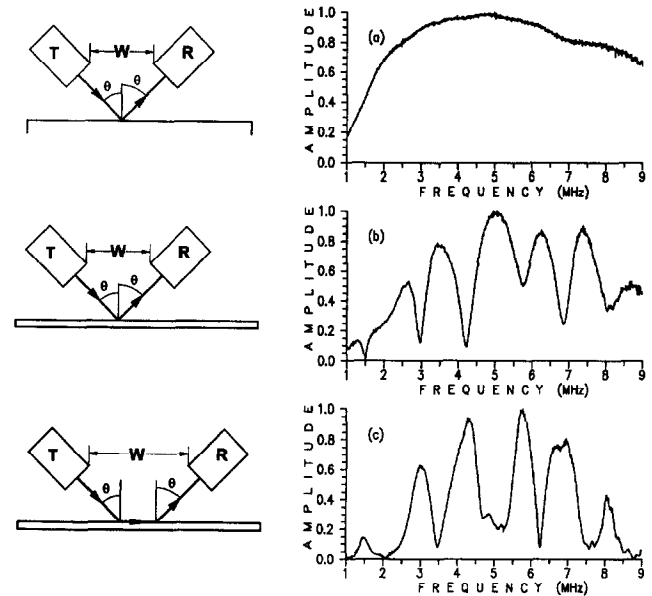


Fig. 1. Reflected wave spectra (right-hand column) for different transmitter–receiver–specimen orientations shown in the left-hand column. For a thick aluminum block reflector no Lamb waves are generated (top figure); for a plate in the focus position, dips in the middle figure correspond to the leaky Lamb waves; for a plate in the defocus position (bottom figure) peaks correspond to the leaky Lamb waves.

ducers then, because of defocusing, the reflected amplitude spectrum changes its shape and magnitude. In this defocused position peaks are observed at the frequencies producing the Lamb waves as shown in Fig. 1c. This is because, when the defocusing is high, the specularly reflected beam cannot reach the receiver but the leaky waves can. That is why we observe peaks in Fig. 1c at the frequency values for which we observed dips in Fig. 1b. Hence, the frequencies corresponding to the Lamb wave modes can be obtained from the dips (Fig. 1b) or peaks (Fig. 1c) of the reflected signal spectra. The Lamb wave speed or the phase velocity can then be obtained from Snell's Law,

$$C_L = \frac{\alpha_0}{\sin(\theta)} \quad (1)$$

where  $C_L$  is the Lamb wave phase velocity,  $\alpha_0$  is the longitudinal wave speed in the coupling fluid (for water it is equal to  $1.49 \text{ km s}^{-1}$ ) and  $\theta$  is the angle of inclination of the transducers, i.e. the angle between the vertical axis and the transducer axis.

If the transducer angle is changed, the corresponding Lamb wave speed is changed, hence the dip positions along the frequency axis vary. Thus, the Lamb wave dispersion curves can be experimentally generated by monitoring the transducer angles and dips of the reflected signal spectra. After selecting a specific Lamb wave mode for scanning, that mode is generated by first setting the transducer angle ( $\theta$ ), then proper defocusing is achieved

by vertically moving the transducers and observing the Lamb wave peaks, and finally the frequency is set at a value corresponding to a Lamb wave peak of interest. The specimen is then scanned with this transmitter–receiver arrangement.

### 3. Experimental results

A five-layer metal matrix composite plate of dimension 80 mm × 1.97 mm is used as the specimen for the Lamb wave scanning. Five layers or plies of SCS-6 fibers in Ti-6Al-4V matrix are oriented in 0° and 90° directions in alternate layers. The top, bottom and middle layer fibers are oriented in the 0° direction, which is along the length direction. The other two plies are in the 90° direction, which is the width direction of the plate. The composite was made by the foil–fiber–foil technique. Some internal flaws were intentionally introduced in the plate during the fabrication process, as shown in Fig. 2. The first and the fifth layers of fibers did not have any flaw. The left part of the second-layer fibers (90°) was coated with boron nitride to impede the formation of good bonding between the fibers and the matrix, as schematically shown in Fig. 2. The fibers in the third layer (0°) were intentionally broken near the middle, as shown in the photograph in Fig. 3 and also shown in Fig. 2. The fourth layer (90°) had two areas of missing fibers, as shown in the photograph in Fig. 4 and schematically in Fig. 2.

Figs. 5, 6 and 7 show the experimentally obtained dispersion curves of the specimen in three different regions. In Fig. 5 dispersion curves of the good region (right-hand side of the plate, see Fig. 2) are shown. Fig. 6 shows the dispersion curves of the bad region (left-hand side of the plate) from the top surface, and Fig. 7 shows the dispersion curves of the same region (left-hand side) from the bottom surface of the plate. Since the debond is not located symmetrically, Figs. 6 and 7 are not identical. Open circles (○) and dots (●) in these figures

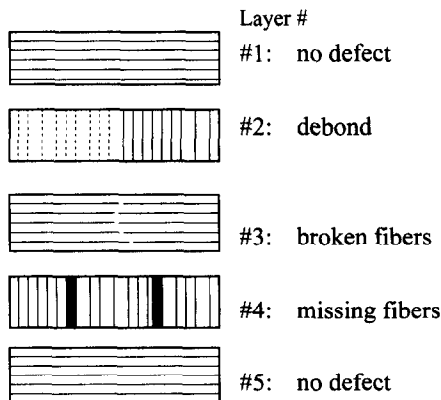


Fig. 2. Schematic of defects in different layers in the five-layer plate specimen.

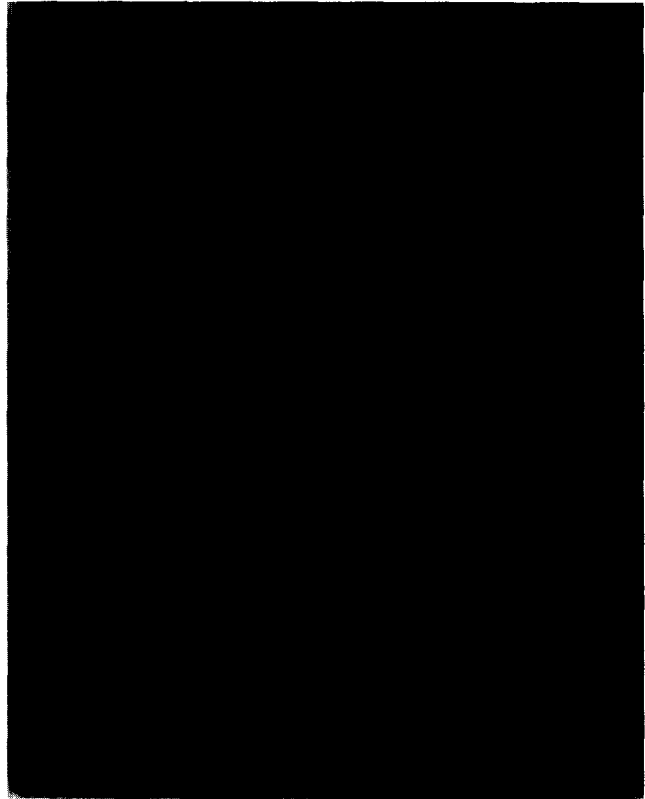


Fig. 3. Photograph of the broken fibers of the third layer, taken before fabricating the specimen.

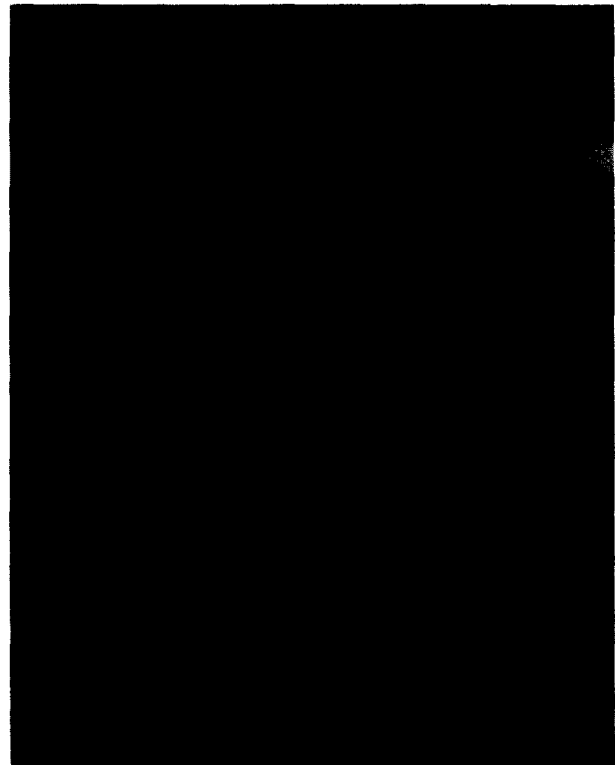


Fig. 4. Photograph of the missing fibers of the fourth layer, taken before fabricating the specimen.

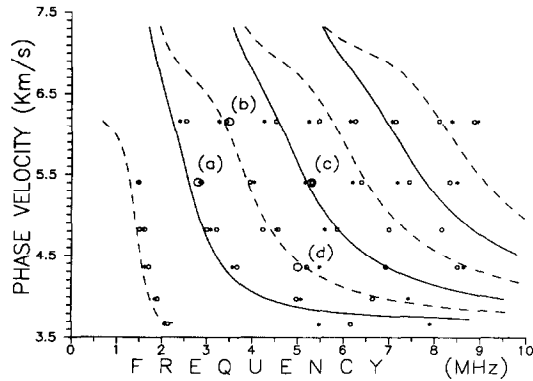


Fig. 5. Experimentally generated dispersion curves in  $90^\circ$  and  $0^\circ$  directions denoted by open circles (O) and dots (●) respectively. Theoretical dispersion curves for a 1.97 mm thick isotropic plate with P-wave speed =  $6.85 \text{ km s}^{-1}$  and SV-wave speed =  $3.65 \text{ km s}^{-1}$  are shown by solid and dashed lines. These plots are for the good region of the plate. Four bigger circles marked as (a), (b), (c) and (d) show the frequency-phase velocity combinations used for generating L-scan images.

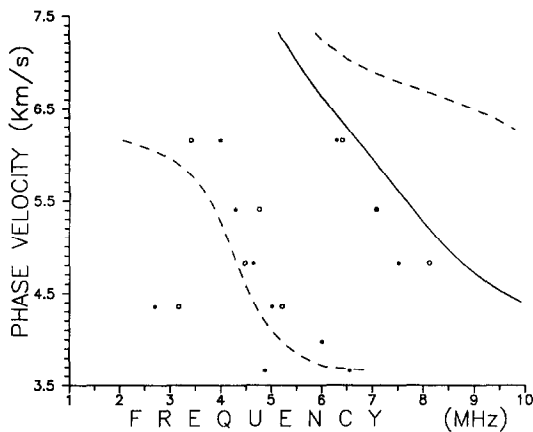


Fig. 6. Same as Fig. 5 but it corresponds to the upper part of the bad region of the plate; for theoretical calculations the plate thickness is taken as 0.66 mm.

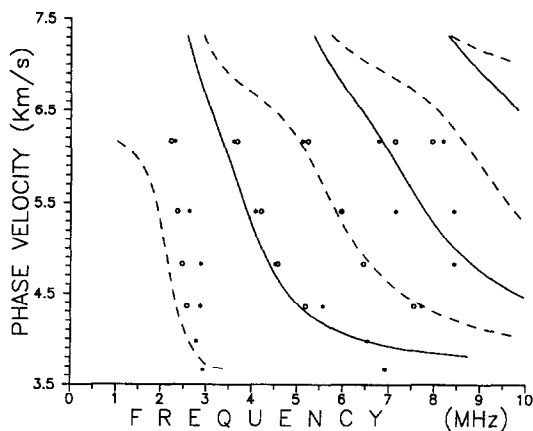


Fig. 7. Same as Fig. 5 but it corresponds to the lower part of the bad region of the plate; for theoretical calculations the plate thickness is taken as 1.31 mm.

correspond to the experimental data points for the Lamb wave propagation in the  $90^\circ$  and  $0^\circ$  directions respectively. Theoretical dispersion curves are computed and plotted by solid and dashed lines in Figs. 5, 6 and 7. To compute theoretical dispersion curves, the plate is assumed to be isotropic and its material properties (average longitudinal and shear wave speeds equal to  $6.85$  and  $3.65 \text{ km s}^{-1}$  respectively) are obtained experimentally. The same material properties are used to compute the theoretical curves in Figs. 5, 6 and 7. Only the plate thickness changes in these three cases. For Fig. 5 this thickness is 1.97 mm, which is the total thickness of the plate; for Fig. 6 the plate thickness is 0.66 mm, the thickness of the plate above the debond, and for Fig. 7 it is 1.31 mm, the thickness of the plate below the debond. In spite of the simplifying assumption of isotropy, the matching between the theoretical curves and experimental data points is very good in Fig. 5, especially for the first four modes,  $S_0$ ,  $A_1$ ,  $S_1$  and  $A_2$  modes. In Figs. 6 and 7 the matching is worse because, in these cases, during the theoretical computation we assumed complete debonding; that is, the top part of the plate that is located above the debond does not affect the bottom part and vice versa, which is not completely true.

Many investigators have studied the relation between the dispersion curves and elastic properties of the plate material and have attempted to obtain these elastic properties by numerically inverting these experimental data [19–28]. However, the emphasis in this paper is not given to the elastic property determination aspect but the capability of imaging the internal defects of the plate. Hence, the relation between the elastic properties and the dispersion curve shapes is not studied in this paper. Instead, different L-scan images with different Lamb wave modes are generated and studied here. Some fundamental theoretical results on the Lamb wave propagation in single and multilayered plates have been presented earlier [1–4] and not repeated here. In the theoretical works it was shown that different Lamb wave modes produce different levels of excitation in various layers in a multilayered composite plate. We try to exploit this phenomenon to generate ultrasonic images of different layers.

The ultrasonic images, generated by scanning the specimen by different Lamb wave modes, are shown in Fig. 8. The images are plotted in 256 grey scales varying from black for no signal to white for the maximum signal. The edge-to-edge distance ( $W$  in Fig. 1) between the two transducers is kept constant at 20 mm for these scans and Lamb waves have been generated in the  $90^\circ$  direction. The transducer-reflector distance is then varied until strong peaks are observed at the critical frequencies in the reflected signal spectrum, as shown in Fig. 1c. More detailed discussion on the transducer and receiver positions relative to the specimen for efficient

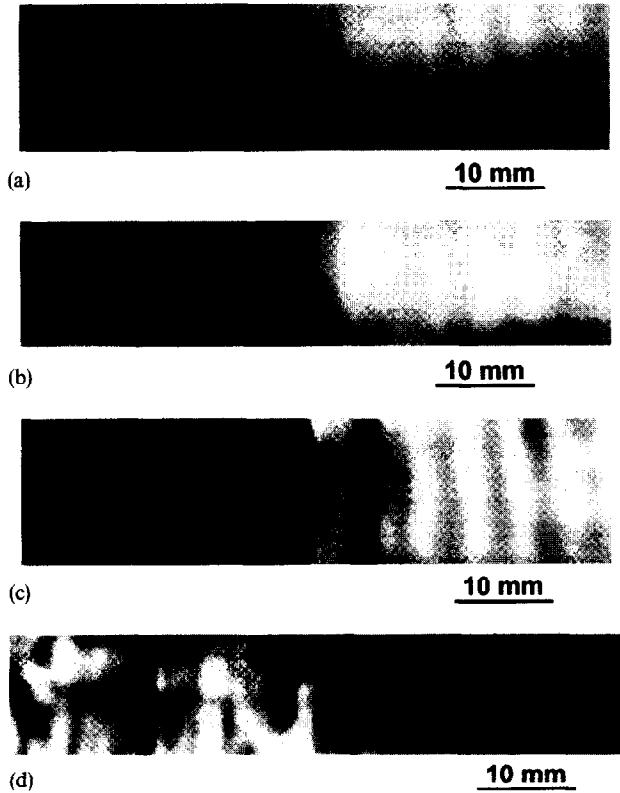


Fig. 8. Different L-scan images of the composite plate. Fig. 8a is generated with the transducer angle  $\theta = 16^\circ$ , and the signal frequency  $f = 2.8$  MHz; for Fig. 8b,  $\theta = 14^\circ$ ,  $f = 3.5$  MHz; for Fig. 8c,  $\theta = 16^\circ$ ,  $f = 5.35$  MHz, and for Fig. 8d,  $\theta = 20^\circ$ ,  $f = 5$  MHz. Figs. 8a and 8c show the second layer debond; the third layer broken fiber zone can be seen in Figs. 8b and 8d and the fourth layer missing fiber regions can be seen in Figs. 8c and 8d.

Lamb wave generation in the specimen is given in Refs. [29–31]. For the image in Fig. 8a the transducer angle is set at  $16^\circ$  (it corresponds to a phase velocity of  $5.41 \text{ km s}^{-1}$ , from Eq. (1)) and the signal frequency is set at 2.8 MHz. This frequency–phase velocity combination is shown by a bigger circle marked by the letter (a) in the dispersion curve plot of Fig. 5. For Fig. 8b the transducer angle is set at  $14^\circ$  (phase velocity =  $6.16 \text{ km s}^{-1}$ ) and the signal frequency is 3.5 MHz, this combination is shown by the circle (b) in Fig. 5. For Fig. 8c, the transducer angle is  $16^\circ$  (phase velocity =  $5.41 \text{ km s}^{-1}$ ) and the signal frequency is 5.35 MHz (see circle (c) in Fig. 5) and for Fig. 8d these are  $20^\circ$  (phase velocity =  $4.36 \text{ km s}^{-1}$ ) and 5 MHz (circle (d) in Fig. 5). Figs. 8a, 8b and 8c are generated by broadband 5 MHz flat transducers of diameter 0.25 inch, while Fig. 8d is generated by slightly focused transducers (focal length 38.1 mm) whose frequency and diameter are the same as before. It is interesting to note that in Fig. 8a the debond zone (dark region on the left-hand side) can be clearly seen; in Fig. 8b a dark band is observed in the central region, in which position fibers of the third layer are broken; in Fig. 8c one dark band can be noticed that

corresponds to the missing fibers of the fourth layer; in addition, Fig. 8c also shows a dark zone for the debond of the second layer. In Fig. 8d, the missing fiber regions are more prominent, and the broken fiber region can also be seen. Clearly, various frequency and transducer angle combinations excited different layers of the plate differently. The combination that is marked by circle (a) in Fig. 5 excited the top and bottom layers strongly, hence we could not see the missing and broken fibers. The combination corresponding to the circle (b) in Fig. 5 excited only the third layer and circle (c) excited the second and fourth layers strongly, circle (d) excited mostly the fourth layer. These experimental observations support the theoretical prediction that various Lamb wave modes excite different layers of a composite plate differently [1–4].

L-scan images are then compared with the conventional C-scan images. Fig. 9 shows three C-scan images generated by 10 MHz (top and middle) and 75 MHz (bottom) focused transducers used in the pulse–echo mode. The transducer axis is positioned normal to the plate specimen. For the top and bottom images the gate position is such that the reflected signals from the middle of the layer are received and the back surface echo is omitted, hence the internal defects should clearly be seen in these two images; for the middle image the back surface echo is recorded. In all these three images the debond can be clearly seen. The missing fibers on the right-hand side can be seen in the top and bottom images, missing fibers on the left-hand side can be faintly seen in the top and bottom images. Broken fibers can

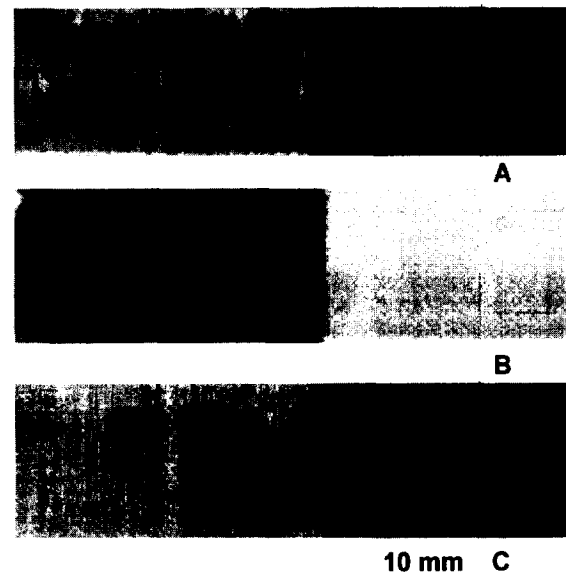


Fig. 9. Conventional C-scan images generated by 10 MHz (top and middle) and 75 MHz (bottom) focused transducers used in the pulse–echo mode. The back surface echo is omitted for constructing the top and bottom images and it is considered for the middle image. Broken fibers and missing fibers can be seen in some of these images but not as clearly as the L-scan images.



Fig. 10. The L-scan image generated by placing the receiver at the null zone, the transducer angle  $\theta = 16^\circ$ , and the signal frequency  $f = 5.35$  MHz. Although  $\theta$  and  $f$  here are the same as those for Fig. 8c, defects here are not as prominent as those in Fig. 8c.

also be faintly seen in all three images at the central region near the good and bad regions' common boundary. In the bottom image,  $0^\circ$  and  $90^\circ$  fiber orientations can be also seen on the left-hand side. Clearly, the L-scan images do not have a very high resolution, unlike the C-scan images generated by high frequency focused transducers. However broken fibers and missing fibers are much more prominent in the L-scan images even with the low frequency transducers.

Next, these L-scan images are compared with an L-scan image that is produced when the receiver is placed in the null zone, as done in Ref. [14], instead of the leaky Lamb wave zone beyond the specularly reflected region, as done here. Fig. 10 shows the image generated by the 5.35 MHz signal with the transducer angle equal to  $16^\circ$ . Hence, transducer orientation and signal frequency for these images are identical to those shown in Fig. 8c. The only difference is that in this case the receiver is located in the null zone, unlike in the previous case. In this figure, only the debond can be seen. In addition to that, many other grey and dark bands can be noted in this image, they are probably due to small thickness variations in different layers – this image is sensitive to the internal defects as well as the plate thickness variation [14].

### Concluding remarks

It is shown in this paper that the Lamb wave scanning technique is superior to the conventional C-scan technique for imaging different types of defects in the internal layers of a multilayered composite plate. The Lamb wave scanning image can show fiber breaks and missing-fiber type defects that cannot be seen very clearly in images generated by the conventional C-scan in the pulse–echo type arrangement, even at very high frequencies. It is also shown that if the receiver is placed at the null zone the defect detection capability is significantly reduced because of the other factors, such as the plate thickness variation, which can affect the null zone position. It is shown here that different layers of the plate can be excited differently not only by various Lamb wave modes but also by a single mode with different phase velocities and frequencies.

### Acknowledgments

This research was supported by the NSF grant CMS-368790 and NATO linkage grant HTECH.LG931353. Drs P. Karpur and T.E. Matikas acknowledge the support under Contract No. F33615-94-C-5213 during the course of this work.

### References

- [1] T. Kundu and M. Blodgett, Review of Progress in Quantitative NDE, Vol. 13, (Eds. D.O. Thompson and D.E. Chimenti) (Plenum Press, New York, 1993) 1343.
- [2] W. Yang and T. Kundu, Proc. 21st Int. Symp. on Acoustical Imaging, 1994, Laguna Beach, California.
- [3] W. Yang and T. Kundu, Wave Propagation and Emerging Technologies, (Eds. V.K. Kinra, R.J. Clifton and G.C. Johnson) (ASME, New York, 1994) AMD-Vol. 188, 109.
- [4] T.W. Taylor and A.H. Nayfeh, J. Acoust. Soc. Am. 91 (1992) 2519.
- [5] D.E. Chimenti and A.H. Nayfeh, J. Appl. Phys. 58 (1985) 4531.
- [6] P.B. Nagy, W.R. Rose and L. Adler, Review of Progress in Quantitative NDE, Vol. 5, (Eds. D.O. Thompson and D.E. Chimenti) (Plenum Press, New York, 1986) 483.
- [7] L.H. Pearson and W.J. Murri, Review of Progress in Quantitative NDE, Vol. 5, (Eds. D.O. Thompson and D.E. Chimenti) (Plenum Press, New York, 1986) 1093.
- [8] W.R. Rose, S.I. Rokhlin and L. Adler, Review of Progress in Quantitative NDE, Vol. 5, (Eds. D.O. Thompson and D.E. Chimenti) (Plenum Press, New York, 1986) 1111.
- [9] A.H. Nayfeh, Review of Progress in Quantitative NDE, Vol. 5, (Eds. D.O. Thompson and D.E. Chimenti) (Plenum Press, New York, 1986) 1119.
- [10] Y. Bar-Cohen and D.E. Chimenti, Review of Progress in Quantitative NDE, Vol. 5, (Eds. D.O. Thompson and D.E. Chimenti) (Plenum Press, New York, 1986) 1199.
- [11] D.E. Chimenti and Y. Bar-Cohen, Proc. 1985 IEEE Ultrasonic Symposium, (Ed. B.R. McAvoy) (IEEE, New York, USA, 1985) 1028.
- [12] R.W. Martin and D.E. Chimenti, Review of Progress in Quantitative NDE, Vol. 6, (Eds. D.O. Thompson and D.E. Chimenti) (Plenum Press, New York, USA, 1987) 815.
- [13] A.K. Mal and Y. Bar-Cohen, Wave Propagation in Structural Composites AMD, Vol. 90, (Eds. A.K. Mal and T.C.T. Ting) (ASME, New York, 1988) 1.
- [14] D.E. Chimenti and R.W. Martin, Ultrasonics 29 (1991) 13.
- [15] Y. Bar-Cohen and D.E. Chimenti, Proc. 15th Symp. Nondestructive Evaluation, Southwest Research Institute, San Antonio, Texas, (1985) 202.
- [16] D.E. Chimenti and C.J. Fiedler, Ceramic Engineering and Science Proceedings, Vol. 8, 11th Annual Conference on Composites and Advanced Ceramic Materials, Cocoa Beach, Florida, 18–23 Jan., (1987) 538.
- [17] J.J. Ditri and J.L. Rose, ASME J. Appl. Mech. 61 (1994) 330.
- [18] N.C. Banik, H.M. Land and J.C. Hamilton, Proc. 1995 ASNT (American Society of Nondestructive Testing) Spring Conference, Las Vegas, USA, 21–23 March, (1995) 227.
- [19] M.R. Karim, A.K. Mal and Y. Bar-Cohen, J. Acoust. Soc. Am. 88 (1990) 482.
- [20] A.K. Mal, M.R. Karim and Y. Bar-Cohen, Mat. Sci. and Eng. A126, (1990) 155.
- [21] A.K. Mal, C.-C. Yin and Y. Bar-Cohen, Composites Engineering 1 (1991) 85.
- [22] B. Tang and E.G. Henneke, II, Mat. Eval. 47 (1989) 928.

- [23] S.I. Rokhlin and D. Marom, *J. Acoust. Soc. Am.* 80 (1986) 585.
- [24] A.H. Nayfeh and D.E. Chimenti, *ASME J. Appl. Mech.* 55 (1988) 863.
- [25] A. Pilarski and J.L. Rose, *J. Appl. Phys.* 63 (1988) 300.
- [26] A.K. Mal, P.C. Xu and Y. Bar-Cohen, *Int. J. Eng. Sci.* 27 (1989) 779.
- [27] V. Dayal and V.K. Kinra, *J. Acoust. Soc. Am.* 85 (1989) 2268.
- [28] V. Dayal and V.K. Kinra, *J. Acoust. Soc. Am.* 89 (1991) 1590.
- [29] P. Karpur, D.M. Benson, T.E. Matikas, T. Kundu and P.D. Nicolaou, *Mat. Eval.*, (1995) in press.
- [30] T. Kundu, P. Karpur, T.E. Matikas and P. Nicolaou, *Proc. 22nd Review of Progress in Quantitative Nondestructive Evaluation Vol. 15*, (Eds. D.O. Thompson and D.E. Chimenti) (Plenum Press, 1995).
- [31] D.M. Benson, P. Karpur, T.E. Matikas and T. Kundu, *Proc. 21st Review of Progress in Quantitative Nondestructive Evaluation, Vol. 14A*, (Eds. D.O. Thompson and D.E. Chimenti) (Plenum Press, 1994) 187.